JOURNAL OF GEOPHYSICAL RESEARCH, VOL. 88, NO. C14, PAGES 9757-9768, NOVEMBER 20, 1983

Analysis of MARSEN *X* Band SAR Ocean Wave Data

R. A. SHUCHMAN,[1] W. ROSENTHAL,[2] J. D. LYDEN,[1] D. R. LYZENGA,[1] E. S. KASISCHKE,[1] H. GUNTHER,[2] AND H. LINNE[2]

Analysis of *X* band SAR imagery collected during the MARSEN experiment indicates that the APD-10 SAR system imaged both range- and azimuth-traveling gravity waves. However, only the near-edge portion of the APD-10 imagery provided reliable spectral wave estimates. Numerous motion artifacts, which manifest themselves as azimuth-oriented streaks, are visible on the data and are believed to be caused by breaking waves. Because of the large platform velocity, the APD-10 SAR data are relatively insensitive to wave enhancement adjustments performed during the processing of SAR signal histories. A modulation transfer function to relate SAR-derived spectra to in situ measurements has been developed. The transfer function is smaller and falls off more rapidly with wave number for azimuth-traveling waves than for range-traveling waves. This is a consequence of the smaller inherent modulation for azimuth-traveling waves and the degraded resolution in the azimuth direction as a result of motion effects and agrees, at least qualitatively, with theoretical predictions.

1. INTRODUCTION

The Maritime Remote Sensing Experiment (MARSEN) was held in the southern part of the North Sea during August and September of 1979, with the primary goal of further developing remote sensing techniques for the retrieval of oceanographic information. The data collected during this experiment included both remotely sensed and in situ measurements. Among the remote sensing instruments used at MARSEN were synthetic aperture radars (SAR's). Both *X* band (3.2 cm) and *L* band (25 cm) SAR data were collected. In this paper we analyze only the data taken with the *X* band SAR.

The purpose of the SAR participation during MARSEN was to better understand the SAR imaging mechanism for ocean waves. This paper presents an analysis of the data collected by APD-10 SAR systems mounted in RF-4 aircraft operated by the United States Air Force of Europe (USAFE). The analysis consisted of (1) examining the effects of scatterer motion on both the wave imagery and the resulting spectra, (2) studying the effect of aircraft heading on the SAR-derived spectral estimates, and (3) performing a comparison between the SAR-derived and surface-measured spectral estimates, including the development of a modulation transfer function (MTF) to relate the two measurements.

Previous experiments with aircraft SAR's have shown that it is possible to detect the dominant wavelength and direction of a surface wave field [*Shemdin et al.*, 1978; *Gonzalez et al.*, 1979; *McLeish et al.*, 1980; *Pawka et al.*, 1980]. The shape of in situ and SAR-derived surface wave spectra, however, show large differences. It is therefore worthwhile to look for a functional relationship between in situ and SAR spectra and to determine the dependence of that relationship on the relevant environmental parameters. This paper presents first results of such investigations. It does not derive them from theoretical assumptions about the mapping mechanism but uses available sea truth to establish quantitative empirical relationships with the SAR image.

In this paper we present first a description of the MARSEN test site and APD-10 system. This is followed by a discussion of the effects of ocean scatterer motion on the resultant SAR images. Next, spectral comparisons between the SAR and in situ measurements are presented. Finally, the development of a modulation transfer function is discussed.

2. DATA DESCRIPTION

The APD-10 is a high-resolution, airborne, side-looking reconnaissance SAR operating at *X* band (3.2 cm). The APD-10 is the radar portion of the UPD-4 system, which includes a ground-based SAR processor. The APD-10 SAR data were recorded on 24-cm film in four subswaths. Each subswath is nominally 4.6 km in width, with an additional 0.46 km overlap between adjacent channels. The nominal operating parameters for the APD-10 at MARSEN are listed in the following table.

APD-10 Radar Parameters for MARSEN Flights

Wavelength	0.032 m
Frequency	9.4 GHz
Polarization	HH (horizontal transmit/horizontal receive)
Pulse width	0.95 μs
FM rate	105 MHz/μs
Average power	70 W
Swath width	18.5 km
Nominal processed resolution	3-m slant range 3-m azimuth
Platform altitude	3.35 km
Near-edge slant range	4.6 km
Far-edge slant range	23.2 km
Near-edge incidence angle	43°
Far-edge incidence angle	82°
Platform velocity	~210 m/s

Synthetic aperture radar is a coherent imaging device that uses the motion of a moderately broad physical antenna beam to synthesize a very narrow beam, thus providing fine azimuthal (along-track) resolution [*Harger*, 1970; *Brown and Porcello*, 1969]. Fine range (cross-track) resolution is achieved by transmitting either very short pulses or longer

[1] Radar and Optics Division, Environmental Research Institute of Michigan (ERIM), P.O. Box 8618, Ann Arbor, Michigan 48107.
[2] Max Planck Institute of Meteorology, Institute of Geophysics, University of Hamburg, Hamburg, West Germany.

Paper number 3C0078.
0148-0227/83/003C-0078$05.00

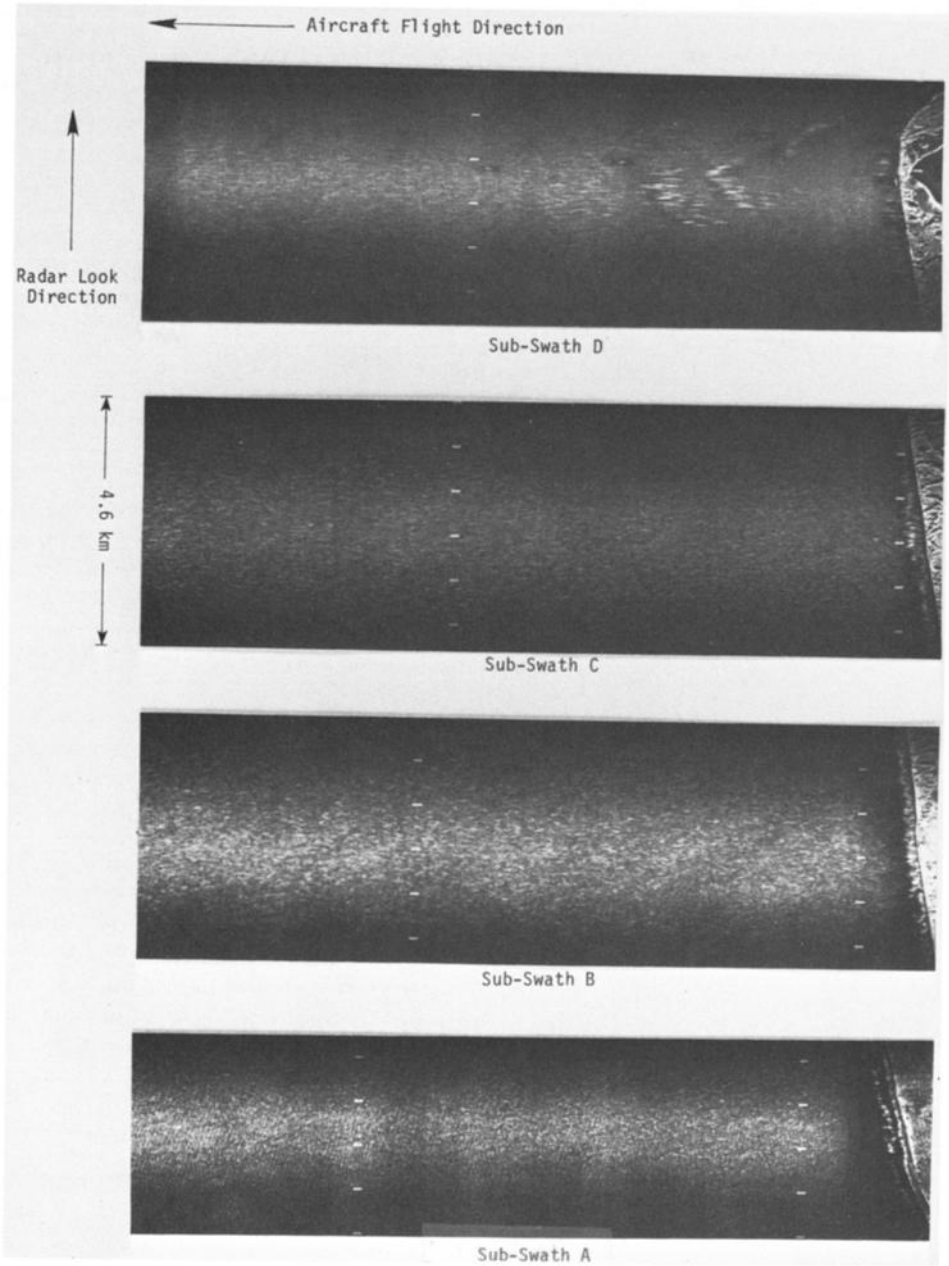

Fig. 1. Example of optically processed APD-10 imagery collected on September 28, 1979, off the coastline of Sylt.

coded pulses that are compressed by matched-filtering techniques into equivalent short pulses.

The APD-10 system is a typical SAR in the sense that the amplitude and phase history information of the returned backscatter is recorded onto photographic film (signal film) aboard the aircraft. These recorded data are utilized by processing the SAR signal film into image film by using standard optical processing techniques [*Kozma et al.*, 1972] and digitizing the SAR image data by using the ERIM Hybrid Image Processing Facility [*Ausherman et al.*, 1975].

Typically, the RF-4 aircraft on which the APD-10 was mounted flew a mission (or line) consisting of a four- or five-sided box or star pattern over the test site. This was done to determine the sensitivity of the SAR look direction for detecting gravity waves. Each individual change of aircraft direction is referred to as a pass of data within a line. The 18.5-km swath of data consists of four subswaths, designated A, B, C, and D (the near-edge subswath being A and the far-edge being subswath D). During the MARSEN experiment, the APD-10 imaged over incidence angles ranging from approximately 40° to 80°. Figure 1 gives an example of the APD-10 data collected off the island of Sylt.

SAR imagery collected during seven separate missions over two test sites were processed at ERIM. These test sites were two instrumented towers in the German Bight in the North Sea. One tower (Nordsee) was located approximately 80 k west of the German island of Sylt; the other tower (Noordwijk) was situated approximately 10 km west of the Dutch coast. A chart showing the general test site area is shown in Figure 2. Presented in Table 1 are the environmental conditions during the seven SAR data collection flights. Note from the table that during the experiment the waves ranged in period from 5.5 to 8.0 and in significant wave height from 1.0 to 1.2 m. The range of winds present varied

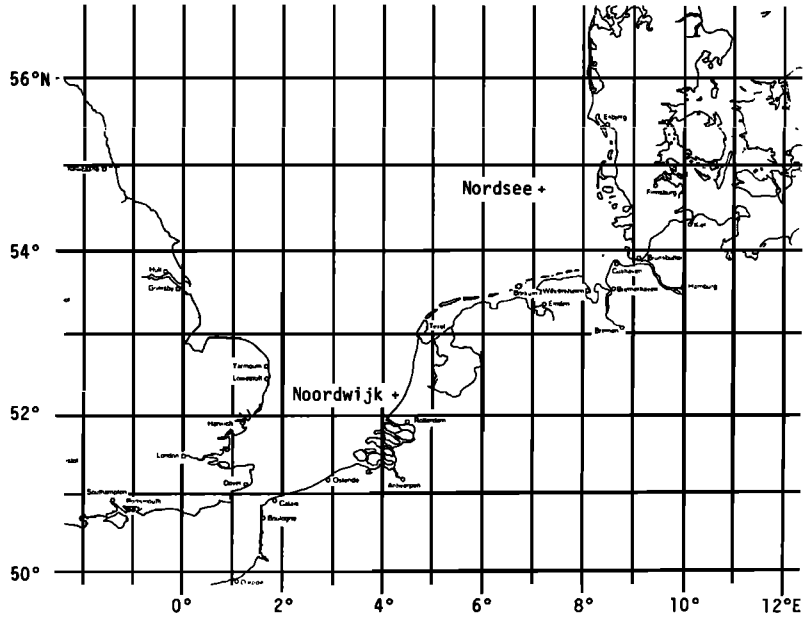

Fig. 2. Chart of the southern portion of the North Sea, showing the location of the Nordsee and Noordwijk research towers.

from 3.5 to 10.3 m/s. Data collected at the Nordsee research tower during lines 7, 10, and 12 are presented in this paper.

The environmental data came from ships and buoys operating near the Nordsee tower. Located at the tower was a wave gauge combined with an electromagnetic current meter (mounted 4 m below the surface) so that the surface elevation and the orbital velocity would be measured at the same time. These data time series were collected by S. Stolte from the 'Forschungsanstalt fur Wasserschall and Geophysik der Bundeswehr,' who made them available to us. These time series were then used to calculate the variance spectrum of the surface waves together with the mean direction for a variety of frequencies. This in situ data was extensively compared to the SAR-derived spectral estimates.

3. Effects of Scatterer Motions

Synthetic aperture radars are sensitive to velocity components present in the imaged scene [*Raney*, 1971]. Effects of wave motions present in SAR imagery may include (1) image displacement, smearing and loss of focus in the azimuth direction, and (2) loss of focus in the range direction. Some of these effects can be removed during processing of the SAR signal histories by making appropriate adjustments to the processor [*Shuchman*, 1981]. The effects that cannot be removed during processing may reduce the detectability of gravity waves and can also influence the wave spectral estimates from the SAR, as discussed in section 4.

Loss of focus in the range direction is due to a rotation of the phase history of the target (i.e., migration through range cells). This loss of focus is proportional to the range velocity and the integration time and can be corrected by a rotation of the lenses in the optical processor, assuming the range velocity of the target is constant during the integration time.

Loss of focus in the azimuth direction can be caused by a constant velocity in the azimuth direction or a changing velocity (i.e., an acceleration) in the range direction. These effects can be corrected by a change in the azimuth focus setting of the processor, assuming that the azimuth velocity and radial acceleration are constant. Since they are both inversely proportional to the platform velocity, these effects are expected to be less important for the APD-10 than for lower-speed aircraft SAR systems.

The effects of image displacement and smearing are not correctable during processing. An image displacement in the azimuth direction occurs as a result of the range velocity of the target. Since the range velocities of the scatterers on the ocean surface vary with position, the resulting differential displacement (velocity bunching) can cause the wave image

TABLE 1. Summary of Environmental Conditions During MARSEN APD-10 Data Collection Flights

			Wave Parameters				Wind Conditions	
Line	Date	Area	Period, s	Frequency, Hz	Propagation Direction*, °true	Height, m	Speed, m/s	Direction†, °true
6	September 28	Noordwijk	8.0	0.125	150	1.0	3.5	330
7	September 28	Nordsee	7.5	0.133	135	1.2	7.2	280
8	September 25	Noordwijk	4.7	0.211	130	1.0	11.8	200
10	September 28	Nordsee	7.5	0.133	133	1.2	7.5	270
11	September 27	Noordwijk	5.5	0.182	150	1.0	8.2	290
12	September 27	Nordsee	7.1	0.141	77	1.0	10.3	290
13	September 27	Noordwijk	5.5	0.182	150	1.0	8.2	330

*Direction waves are propagating towards.
†Direction wind is coming from.

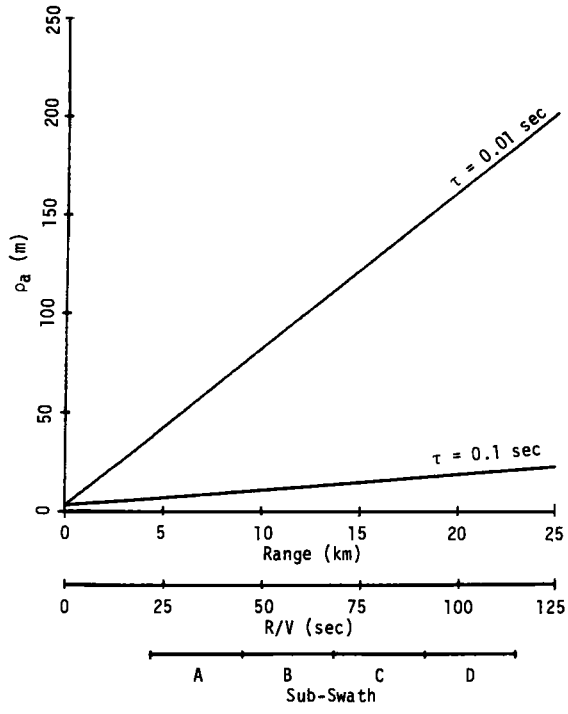

Fig. 3. Azimuth resolution as a function of radar range for the APD-10 system, assuming two values of the coherence time (τ).

to be either enhanced or degraded, depending on the viewing geometry and the SAR system parameters [*Alpers et al.*, 1981]. This effect is probably not extremely important for the APD-10 data collected at MARSEN because of the relatively large incidence angles and the high velocity of the platform.

When a given resolution cell contains scatterers moving at different range velocities, each scatterer is displaced in azimuth by a different amount, resulting in a smearing or loss of resolution in the azimuth direction. This effect is particularly important in breaking seas and is illustrated by the streaked image features appearing prominently in the MARSEN SAR imagery. These observed streaks will be discussed in detail later in this section. This loss of resolution is not recoverable during processing and appears to be the primary limiting factor in the ability of the APD-10 to image ocean waves at MARSEN.

The effect of a range of velocities δV_r within a resolution cell is equivalent to the coherence time effect discussed by *Raney* [1980], with a coherence time (τ) given by

$$\tau = \frac{\lambda}{2\delta V_r} \tag{1}$$

X band coherence times on the order of 10^{-2} to 10^{-1} s have been measured for conditions similar to those encountered at MARSEN [*DeLoor and Hoogeboom*, 1982]. The effective azimuthal resolution is given by

$$\delta x = \left[\left(\frac{\lambda}{2\beta}\right)^2 + \left(\frac{\lambda R}{2V\tau}\right)^2\right]^{1/2} \tag{2}$$

where λ is the radar wavelength, β is the antenna beamwidth, R is the range, and V is the platform velocity. The resolution is plotted versus range for the APD-10 system for both $\tau = 10^{-2}$ s and $\tau = 10^{-1}$ s in Figure 3. Note that for $\tau = 10^{-2}$ s, the resolution becomes equal to the wavelength of the dominant waves at MARSEN (i.e., ~90 m) at about the middle of swath B. Thus azimuth-traveling waves of this length would not be imaged in swath B under these conditions. Range-traveling waves are not influenced by this loss of azimuth resolution and are therefore imaged at larger ranges. This effect is in fact observed in the APD-10 imagery, as shown in Figure 4.

A. *Processor Adjustments*

Previous studies using aircraft SAR data have shown that the visibility or detectability of gravity waves is often sensitive to motion compensation adjustments made during the processing of SAR signal histories [*Shuchman*, 1981; *Kasischke and Shuchman*, 1981]. An aspect of this study

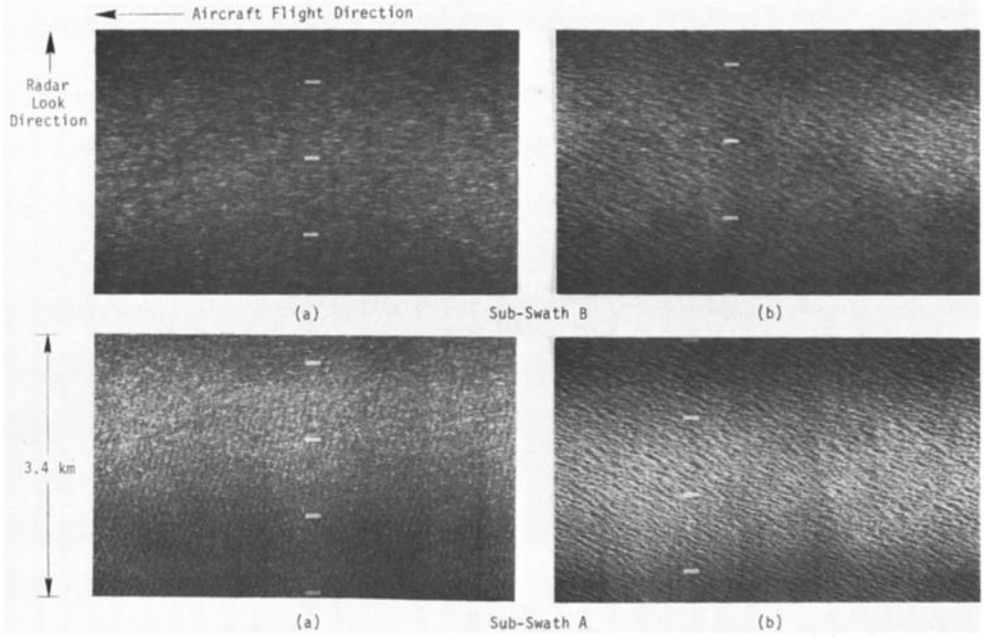

Fig. 4. Examples of APD-10 wave imagery from line 7, subswaths A and B for azimuth-traveling (a), and range-traveling waves (b).

was to determine if SAR data collected by the APD-10 system are also sensitive to these motion compensation adjustments.

Two SAR processor adjustments were evaluated by using the MARSEN APD-10 data set to determine if the SAR wave imagery could be improved. These processor adjustments include (1) an azimuth focus shift to correct for azimuth velocities and range accelerations and (2) a telerotation adjustment to correct for range walk. These two processing adjustments were varied during the optical processing so as to determine the sensitivity of SAR data collected by the APD-10 system to focus adjustment techniques. These focus adjustments are inversely proportional to the velocity of the SAR platform. Since the RF-4 has a high platform velocity (~210 m/s), the adjustments, if necessary, are probably quite small and the effect on SAR imagery quite subtle.

Azimuth focus shifts were used on SAR data for waves traveling perpendicular to the radar line of sight, and range telerotation adjustments were used for waves traveling parallel to the radar line of sight. For intermediate cases a combination azimuth focus shift and range telerotation adjustment was used. For calculation of the azimuth focus shifts, the range walk corrections, and the combination azimuth and range corrections, a family of velocities was used that ranged from a stationary target to twice the phase velocity of the gravity waves present. The direction of wave propagation was not assumed, thus positive and negative velocity corrections were tested. This resulted in nine velocity values being used for each of the enhancement tests. In all, a total of seven passes of imagery from three lines were evaluated.

To measure wave visibility, a crest-to-trough contrast measurement called a peak-to-background ratio (PBR) was used. A PBR is obtained by measuring the peak intensity of the two-dimensional Fourier transform of the SAR wave image and dividing that peak by the lowest intensity at the same wave number [*Kasischke and Shuchman*, 1981].

Five separate PBR measurements were obtained for each telerotation, focus shift, or combination setting. By running a statistical analysis of variance test [*Sheffe*, 1959] on the PBR's from a set of focus adjustments, a determination was made as to whether the adjustments resulted in significantly higher PBR's, hence improved wave visibility on the SAR imagery.

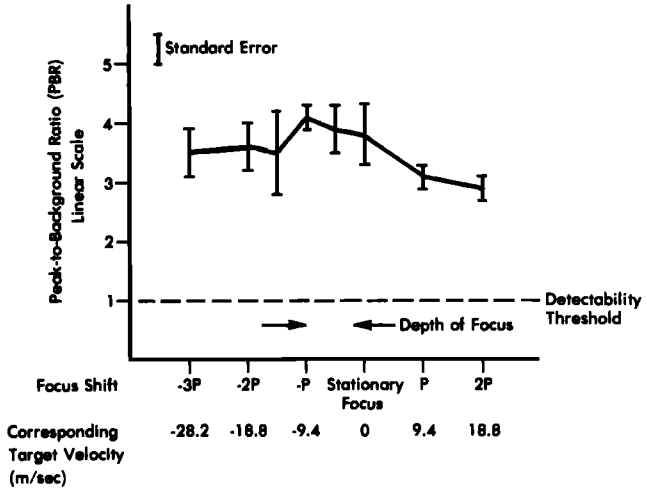

Fig. 5. Wave peak-to-background ratio as a function of azimuth focus shifts for line 7, pass 4 data.

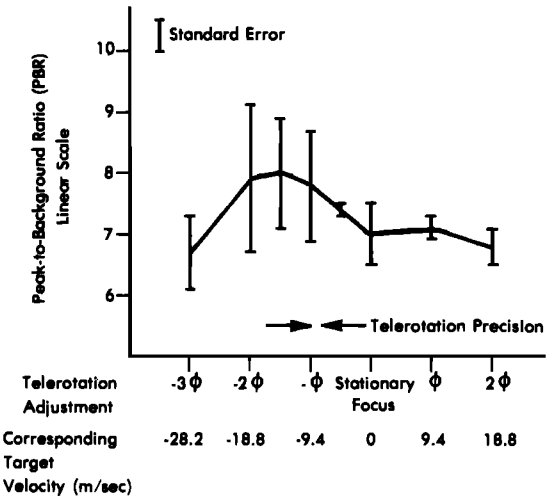

Fig. 6. Wave peak-to-background ratio as a function of range telerotation adjustments for line 7, pass 2 data.

Figure 5 represents a graph of the PBR versus azimuth focus setting for line 7, pass 4 data. Figure 6 is a similar graph, which shows the relationship of PBR to range focus adjustment. The data utilized in this example is from line 7, pass 2. The results of the azimuth focus shift and range telerotation adjustments indicated the APD-10 *X* band SAR imagery was relatively insensitive to azimuth focus shifts and somewhat sensitive to range telerotation adjustments. This result is due to the high platform velocity of the F-4 aircraft (210 m/s). In most cases the distribution of the nine velocity settings versus PBR (on each of the three types of enhancement) gave an indication as to which direction the waves were traveling because the curve was skewed in that direction.

B. Azimuth Streaking

The APD-10 SAR data collected over both shallow and deep water shows numerous bright streaks in the along-track or azimuth direction. These streaks become longer and more apparent as the range or incidence angle increases, as shown in Figure 7, and frequently obliterate the wave images in the further subswaths. They are apparently related to the 'sea spike' phenomenon noted in conventional radar observations of the ocean at large incidence angles [*Long*, 1974; *Lewis and Olin*, 1980]. These features appear more prominently at far range because the Bragg scattering background falls rapidly with increasing incidence angle while the return from the streaks remains nearly constant. An analysis of this phenomenon is presented in the companion paper [*Lyzenga and Shuchman*, 1983], and the implications of this streaking for the wave imaging process are described in this section and section 4B.

The effects of these features on the SAR image spectrum is to add a background component that has a spectral shape determined by the length, or resolution, of the streaks. If the streaking is not so severe as to completely obliterate the wave image, this background component can be removed by the methods discussed in the following section. However, when the streak lengths become comparable to the azimuth component of the wavelength, the wave information is effectively lost. This streaking, along with the loss of azimuth resolution of the wave component itself, limits the range of incidence angles over which wave imagery can be

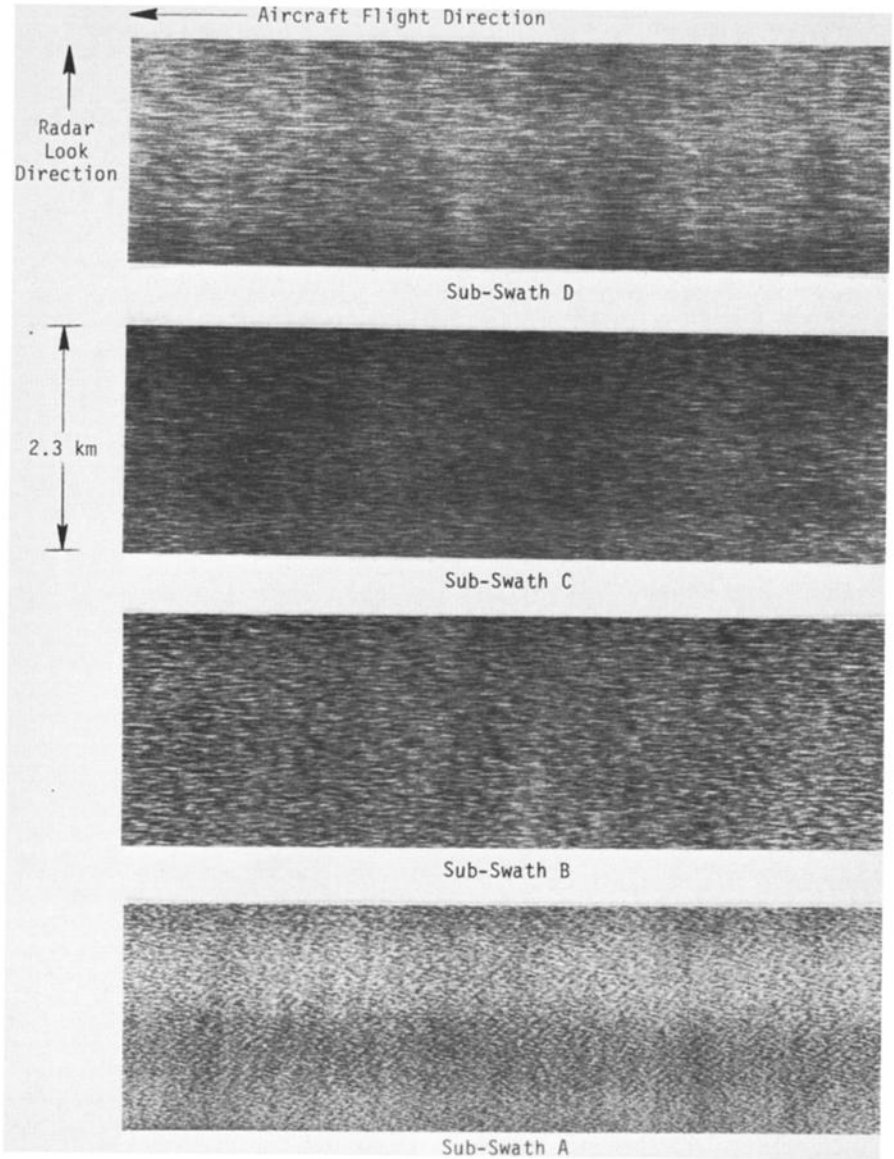

Fig. 7. Optically processed APD-10 imagery for a portion of all four subswaths for line 12, pass 3. Note the streak length increases with range.

obtained, as discussed in section 4B, below. The relationship between the characteristics of the streaks and the SAR modulation transfer function for ocean waves is currently under investigation.

In addition to their negative impact on the wave imaging process, these features may be useful indicators of the sea state. A comparison of the frequency or number density of the streaks with in situ measurements of wave breaking [*Longuet-Higgins and Smith*, 1983] is under way and will be reported in the near future.

4. SAR vs. In Situ Spectral Comparisons

This section of the paper compares the SAR-derived spectral estimates with in situ oceanographic measurements. The surface-based spectra were obtained by processing data collected by a wave gauge and current meter which were operating during the SAR overflights at the Nordsee Tower. Recall that the SAR-derived spectra are in wave number space, while the surface-based spectra are given in frequency. Prior to making any comparisons between the two, one estimate has to be converted to the other's domain. For this study the surface-measured spectral estimates were converted to wave number space assuming a dispersion relationship of the form

$$f = \left(\frac{g}{\lambda 2\pi} \tanh kd\right)^{1/2} \tag{3}$$

appropriate for intermediate water depths where f is the wave frequency, g is the acceleration of gravity, λ is the wavelength, k is the wave number ($2\pi/\lambda$), and d is the water depth (assumed to be 30 m).

The SAR data used in this study were collected during lines 7, 10, and 12. These SAR signal films were optically processed into image film by using the ERIM Precision Optical Processor (POP). These image films were digitized with 3-m samples by the ERIM Hybrid Image Processing Facility (HIPF), described by *Ausherman et al.* [1975]. Digital spectral estimates are produced from 512 × 512 pixel (1.5 × 1.5 km) subsets of these digital data. Prior to spectra

TABLE 2. SAR Versus Sea Truth Comparisons

Line	Pass	Aircraft Heading, °true	Surface Measured*			SAR Derived		Observed Differences	
			f, Hz	λ, m	θ, °true	λ, m	θ, °true	λ, m	θ, °true
7	Sylt	297	0.133	86	135	86	133	0	−2
	1	283				92	131	+6	−4
	2	056				60	109	−26	−26
	3	191				86	131	0	−4
	4	327				86	130	0	−5
	5	102				109	147	+23	+12
10	1	283	0.133	86	133	99	148	+13	+15
	2	056				91	129	+5	−4
	3	191				103	129	+17	−4
	4	327				109	152	+23	+19
	5	102				130	152	+44	+19
12	Sylt	297	0.141	78	77	75	52	−3	−25
	1	283				75	43	−3	−34
	2	056				75	78	−3	+1
	3	191				89	61	+11	−16
							Mean	7.6	−4.1
							Standard Deviation	16.6	16.8

*The surface-measured wavelengths were derived assuming a water depth of 30 m.

generation, these subsets undergo corrections for slant range distortion and to remove long-period variations of intensity in both range and azimuth. The data is also smoothed by using a 4 × 4 pixel weighted filter, which reduces the coherent speckle found in the imagery and also reduces the number of samples by a factor of 2 in each dimension. Two-dimensional fast Fourier transforms (FFT's) were performed on each 256 × 256 cell subsection to yield raw directional wave number spectra with a Nyquist wave number of 0.52 m^{-1}. The raw spectra were smoothed by replacing each value with the average of the surrounding 5 × 5 cell. The approximate number of degrees of freedom for the resulting spectrum is 142 [*Kinsman*, 1965], and the 99% confidence limits are ±1.5 dB [*Jenkins and Watts*, 1968].

The surface measurements used for comparison with the SAR were obtained at the Nordsee tower, coincident with the SAR flights. These measurements were made by a wave gauge coupled with an electromagnetic current meter so that simultaneous measurement of surface elevation and orbital velocity could be made with a sampling rate of 2 Hz. From these time series we were able to calculate the variance spectrum of the surface waves as well as the mean direction for 128 intervals equally spaced from 0 to 1 Hz, following the method of *Forristall et al.* [1978]. Ten of these spectra were averaged to increase the degrees of freedom to about 30.

Presented in Table 2 is a comparison of the dominant SAR-derived (subswath A) and surface-measured spectral estimates for lines 7, 10, and 12. Line 12 was flown on September 27 from 0840 to 0917 GMT. The surface wind speed during this flight was approximately 10 m/s, from a direction of 290°. The surface-measured wave spectrum had a peak frequency of 0.141 Hz propagating at 77°, which corresponded to a fully developed wind-generated sea. Because of the recent passage of a storm, the difference between surface wind and wave directions during the flight was 33°, which results in a change of wave direction with frequency so that the higher frequencies become more aligned with the wind [*Hasselmann et al.*, 1980; *Gunther et al.*, 1981]. Lines 10 and 7 were flown on September 28 from 0938 to 1035 and 1121 to 1222 GMT, respectively. The surface conditions during lines 10 and 7 were very similar, with surface wind speeds and directions of 7.5 and 7.2 m/s and 270° and 280°, respectively. The surface wave conditions were also almost identical, with each having a peak frequency of 0.133 Hz and directions of 133° and 135° for lines 10 and 7, respectively. This wave frequency is well beneath the Pierson-Moskowitz frequency for the prevailing wind speed. Upon examination of the surface-measured spectrum and the wind conditions prior to the flights, it was concluded that these conditions represent the typical situation of a wave spectrum after a recent decrease of the local wind speed.

From Table 2 it appears that the APD-10 SAR operating at MARSEN was able to detect ocean gravity waves with an accuracy of 16.6 m in length and 16.8° in direction once the mean biases were removed. Consistent with past studies the SAR-derived waves were slightly longer than the in situ measurements. The question of SAR-derived spectral estimate accuracy as a function of radar look direction will be discussed in more detail below.

A. *Wave Detectability vs. Radar Look Direction*

As previously mentioned, multisided SAR flight patterns were flown during MARSEN. An example of this pattern is shown in Figure 8 for line 7. This figure is a diagram of the

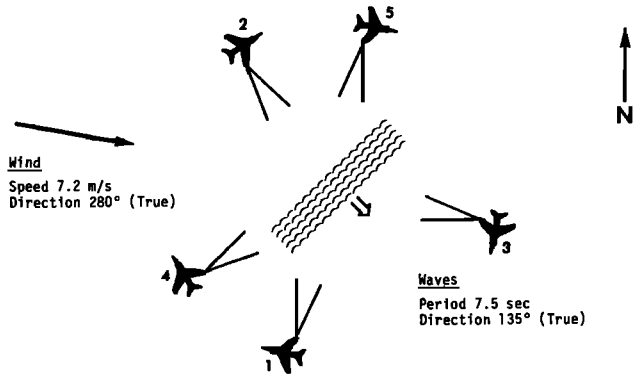

Fig. 8. SAR collection geometry for line 7, passes 1–5. Also shown are the surface environmental conditions during the data collection.

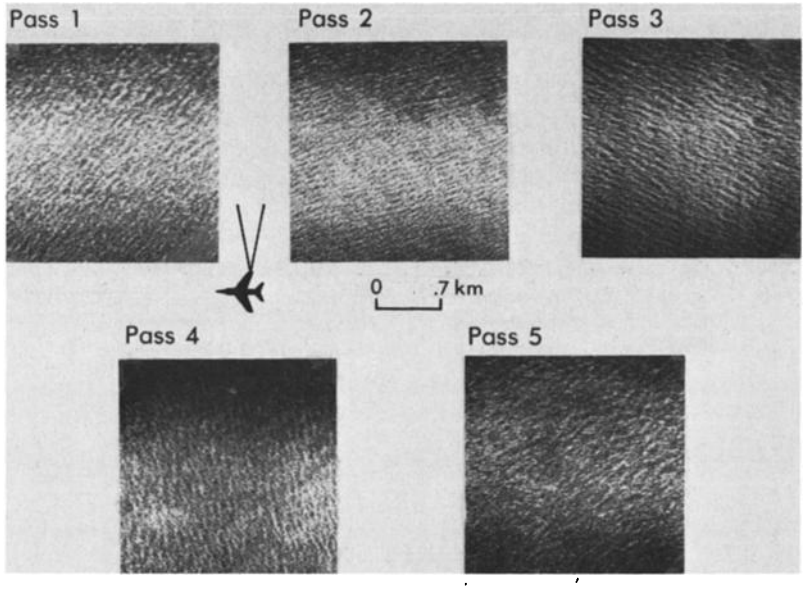

Fig. 9. Optically processed APD-10 gravity wave imagery from subswath A for line 7, passes 1–5.

collection geometry for five passes from line 7. Figure 9 shows imagery for a section from each of these five passes. Figure 10 presents two-dimensional contour plots of the FFT's produced for each of the passes described in the previous section. Each contour on these plots represents a 3-dB (50%) decrease in spectral intensity from the previous one. On the plots the azimuth direction is the horizontal axis, and the range direction is the vertical axis. The SAR-derived dominant wave is represented by the highest contour on these plots.

Past studies in SAR imaging of ocean waves have shown that range-traveling waves are more clearly imaged than azimuth-traveling waves [*Shemdin et al.*, 1978]. It should be noted that the waves in these past studies consisted of swell,

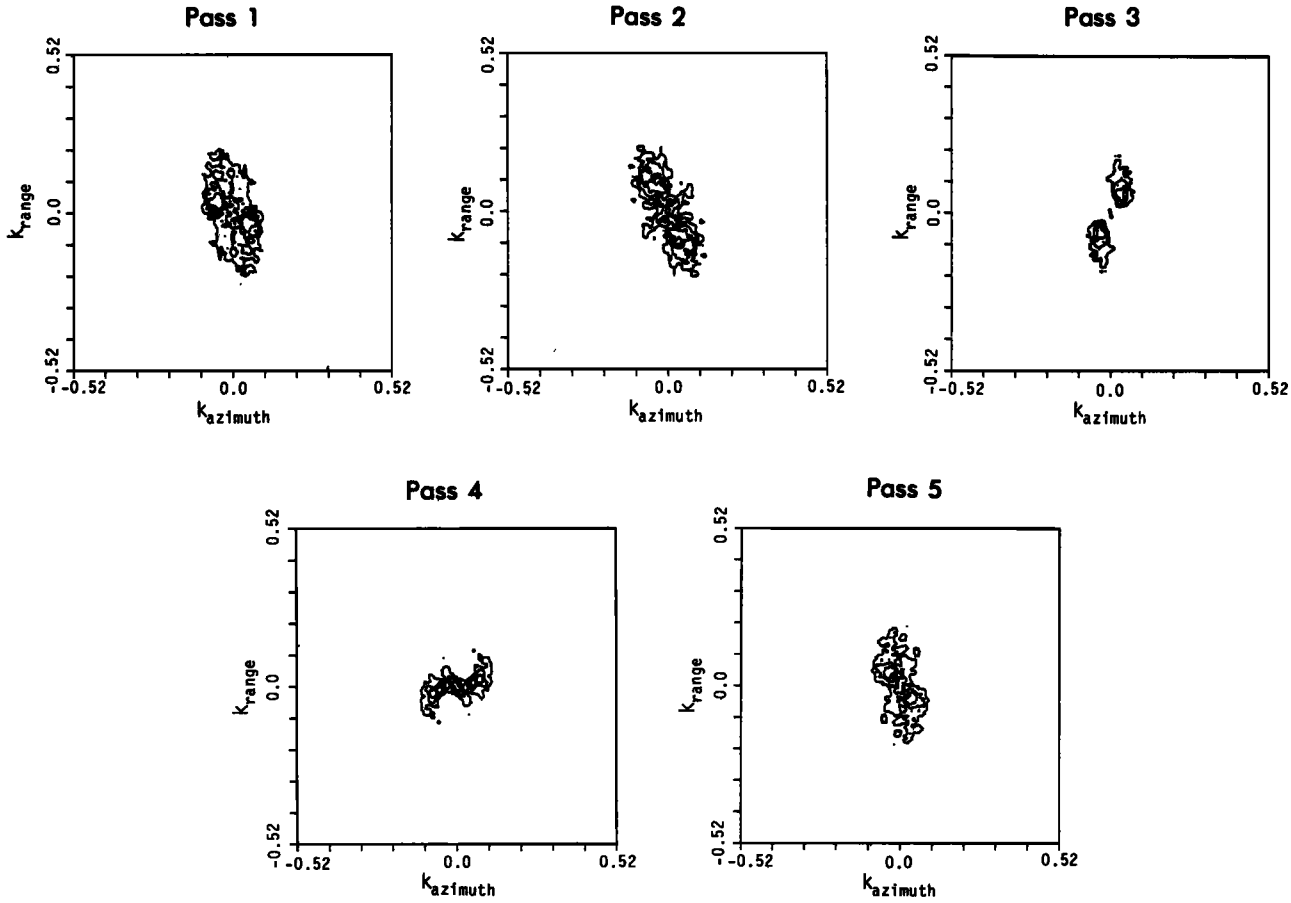

Fig. 10. Two-dimensional contour plots of the fast Fourier transforms (FFT's) produced from the digitized imagery shown in Figure 9.

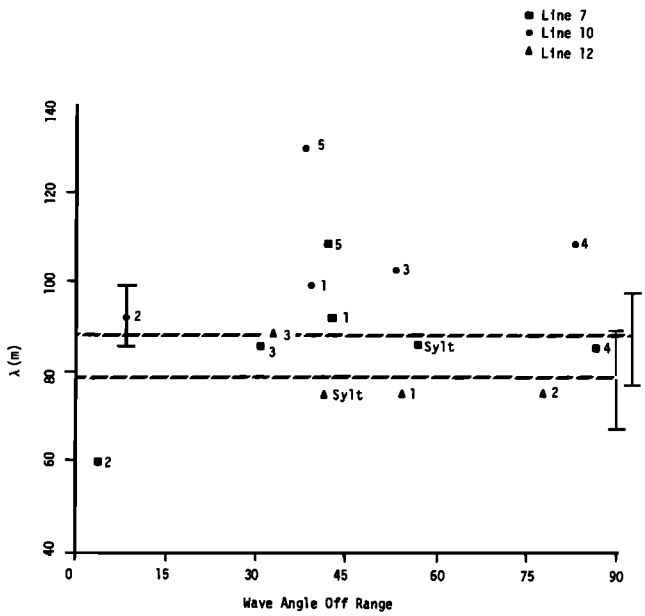

Fig. 11. SAR-derived wavelength estimates (λ) versus wave angle off range for lines 7, 10, and 12. Included on the plot as dashed lines are the wavelength estimates based on surface measurements. The error bars indicate the accuracy for the surface measurements and a single pass of SAR data. These error bars were based on the resolution of the spectra from both instruments.

not wind-generated waves as were present at MARSEN. The accuracy of SAR-derived spectral estimates as a function of the radar look direction, however, has not been rigorously studied. To address this question, the SAR-derived spectral estimates summarized in Table 2 were plotted versus the relative look angle from purely range-traveling waves, based on surface measurements for both wavelength and direction. These plots are shown in Figures 11 and 12, respectively. Also shown on the figures are the surface-measured waves for each line. Note that these plots ignore up or downwave differences. By displaying the data in this coordinate system, it was hoped that any systematic or periodic bias in the SAR-derived spectral estimates caused by changing look direction could be ascertained. Examination of Figure 11 shows that the wavelength estimates from the SAR appear to be randomly scattered as a function of radar look direction. With the exception of four points, the wavelength estimates are all within 20 m of the surface-measured values. It is interesting to note the variability between lines 7 and 10, which were flown with nearly identical geometries. This suggests that the variability of the SAR wavelength estimate at a given look direction is on the order of the variability of SAR-derived wavelength estimates as a function of look angle.

Examination of Figure 12 shows similar results to Figure 11, that is, the variability between the SAR-derived wave directions for lines 7 and 10 is on the order of the variability of the directional estimates across the whole range of angles. The line 12 estimates shown on Figure 12 do not appear very accurate. Three more range-traveling passes show a monotonic increase in directional difference to the surface-measured values with increasing angle off range, but the azimuth-traveling pass is very close to the surface-measured value.

Several points should be made about Figures 11 and 12. We have assumed the aircraft headings, as recorded in the flight log, to be correct. Past experience has shown this assumption to be a possible source of error; if that is true in this case, the results of Figure 12 will change. We have also assumed a constant water depth of 30 m; if not valid, this assumption would alter the surface-derived values in Figure 11 as a function of pass location (i.e., water depth). Finally, we have based this analysis on a limited set of passes with somewhat random look angles with respect to wave propagation direction. To adequately perform this sort of analysis, wave imagery should be available with 10° intervals from purely range-traveling to purely azimuth-traveling waves.

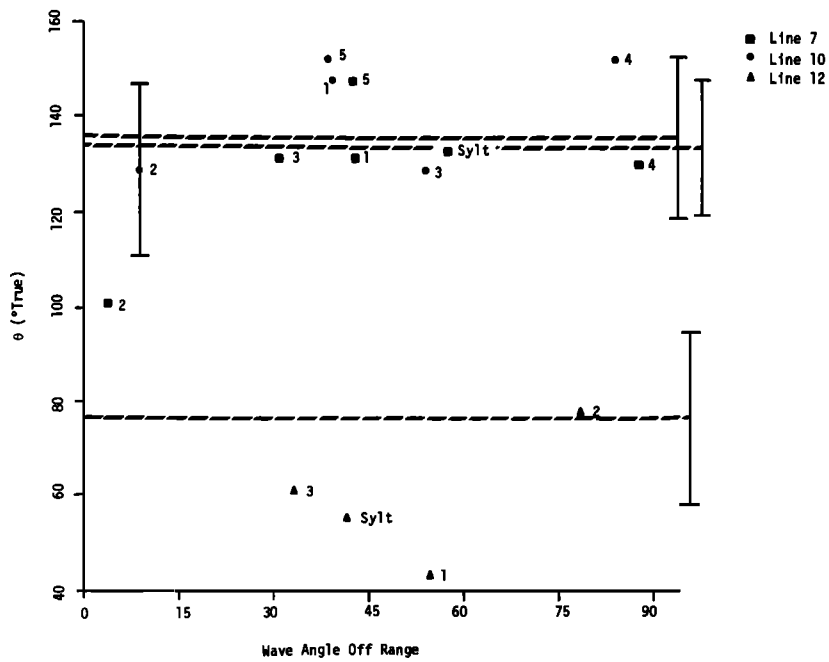

Fig. 12. SAR-derived directional estimates (θ) versus wave angle off range for lines 7, 10, and 12. Included on the plot as dashed lines are the directional estimates based on surface measurements. The error bars indicate the directional spread of the surface measurements and the average −3-dB contour width of the SAR-derived spectra.

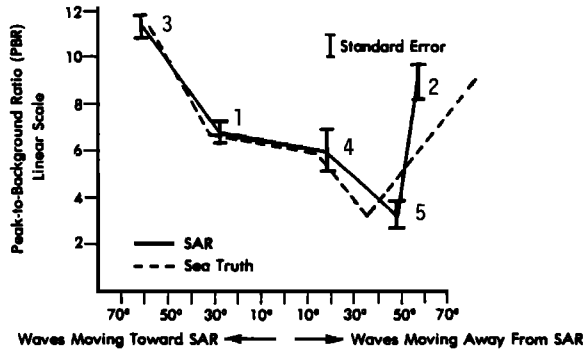

Fig. 13. Wave peak-to-background ratio versus radar look direction for line 7, passes 1–5. Refer to Figure 8 for the collection geometry and Figure 9 for representative imagery from each pass.

Ideally, this data would be gathered over a full 360°. This type of data set would be useful in evaluating and developing SAR wave imaging theories. Recent examination of Marineland SAR data, where more data points were available than MARSEN, shows that azimuth-traveling waves are consistently imaged as being longer than range-traveling waves [*Shuchman et al.*, 1983].

The sensitivity of wave visibility with respect to radar look direction was evaluated by using the PBR method described in section 3A. The PBR's from the enhancement tests consistently showed highest wave contrast resulting from SAR images of range-traveling waves and lower values resulting from azimuth waves. It has been previously reported [*Teleki et al.*, 1978] that SAR's, particularly when operating at *L* band, will image range-traveling waves more clearly than azimuth waves. Using line 7 data, PBR measurements were obtained from subswath A in the same general location around the Nordsee Tower for each of the five passes. Figure 13 shows a graph of the PBR value obtained versus the orientation of the waves with respect to the radar look direction (see Figure 8 for the collection geometry). Note that two curves are presented on the graph: one indicates PBR versus the sea truth direction, while the other is PBR versus the radar-derived value. A zero-degree value on the graph indicates azimuth-traveling waves. Analysis of Figure 13 indicates that (1) SAR images range-traveling waves more clearly than azimuth-traveling waves, (2) SAR images waves more clearly when they are moving toward the SAR than when they are moving away from the SAR (i.e., pass 1 versus 5 or 2 versus 3), and (3) the APD-10 *X* band SAR imaged gravity waves during line 7, regardless of radar look direction.

B. *Wave Detectability vs. Incidence Angle*

The effect of varying incidence angle on the detection of gravity waves was also evaluated by using this APD-10 data set. Recall that the APD-10 system collects an 18.5-km swath in four subswaths where the incidence angle varies from 43° to 82°. Figure 14 shows contour plots of FFT's obtained from each of the four subswaths for pass 3 from line 12. The corresponding imagery was previously shown as Figure 7. It is apparent that an azimuth-oriented artifact becomes more pronounced as the incidence angle or range to the ocean surface increases (i.e., from subswath A to subswath D). In fact the spectra in swaths C and D are completely dominated by this artifact. Over this same interval, the gravity waves of interest become less visible, and the azimuth-oriented streaks can lead to a perceived range-traveling wave. Thus, because of these streaks on the MARSEN APD-10 imagery and the relative fading (decreased contrast) of imaged gravity waves with range, accurate wave estimates can only be extracted from subswath A.

C. *Modulation Transfer Function*

As part of the MARSEN data analysis an attempt was made to establish an experimental relationship between the variance spectrum of the radar image $S(k)$ and the wave height spectrum $W(k)$. This relationship is most likely nonlinear, in the sense that it is dependent on the total shape of $W(k)$ instead of the value at one single k value. However, it may be possible to describe the spectral shape by a small set of characteristic properties (for example, the averaged frequency, direction, and spectral width) and use these as parameters in the mathematical description of the mapping from $W(k)$ into $S(k)$ or vice versa.

The spectrum of the SAR image includes both the desired wave information as well as contributions caused by SAR system noise, speckle effects, and imaged point scatterers. Thus, in order to provide a more meaningful comparison with in situ measured wave height spectra, the SAR image spectra were partially corrected by subtracting off the components caused by speckle, system noise, and imaged point scatterers. The sum of these three components was estimated by examining the spectrum in the wave number quadrants not containing the dominant wave and by assuming symmetry in the background spectrum with respect to the k_x and k_y axes. That is, the corrected image spectrum is given by

$$S(k_x, k_y) = I_m(k_x, k_y) - I_b(k_x, k_y) \quad (4)$$

where $I_m(k_x, k_y)$ is the (total) measured spectrum, and $I_b(k_x, k_y)$ is the background spectrum estimated from $I_m(-k_x, k_y)$ or

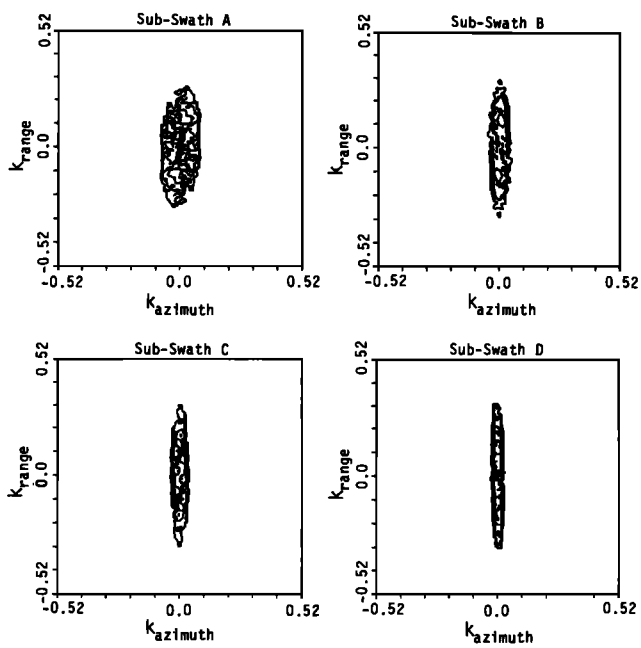

Fig. 14. Two-dimensional contour plots of the fast Fourier transforms (FFT's) produced for all four subswaths from Line 12, Pass 3 data. Refer to Figure 7 for the corresponding optically processed imagery.

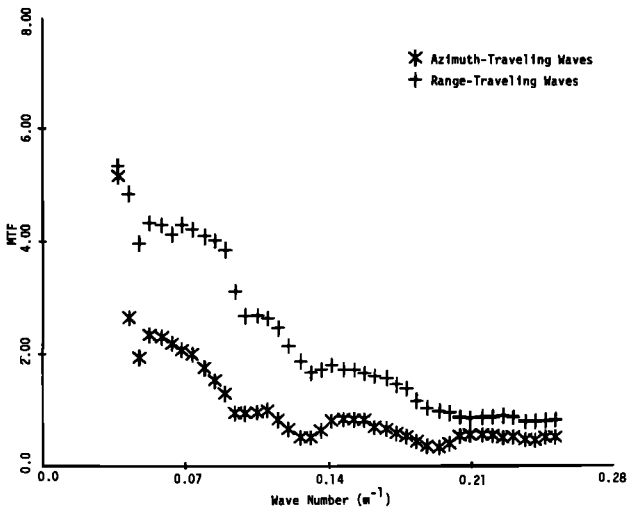

Fig. 15. One-dimensional modulation transfer function (m') as a function of wave number for a nearly azimuth-traveling and a nearly range-traveling wave.

$I_m(k_x, -k_y)$. This corrected spectrum may be written in polar form (i.e., $S(k, \theta)$) and then converted into a one-dimensional spectrum

$$S(k) = k \int_0^{2\pi} S(k, \theta)\, d\theta \tag{5}$$

using the coordinate transformation

$$k = (k_x^2 + k_y^2)^{1/2} \tag{6}$$

and

$$\theta = \tan^{-1}(k_y/k_x) \tag{7}$$

and this quantity was then compared with the in situ measured wave height spectrum $W(k)$ by calculating the modulation transfer function.

The terms 'modulation transfer function,' 'mapping transfer function,' and just 'transfer function' are used somewhat ambiguously in the radio-oceanographic literature to denote the relationship between the ocean wave information measured by a radar and the physical surface descriptions usually measured by conventional in situ instruments.

In the linear modulation theory developed by *Keller and Wright* [1975] and *Alpers and Hasselmann* [1978], the radar return for a monochromatic ocean wave is written as

$$P = P_0 \left[1 + \frac{mV_0}{C} \cos(\Omega t + \phi)\right] \tag{8}$$

or

$$P = P_0[1 + |R|\zeta_0 \cos(\Omega t + \phi)] \tag{9}$$

where m is the modulation transfer function defined by Keller and Wright, R is the modulation transfer function defined by Alpers and Hasselmann, V_0 is the maximum orbital velocity of the wave, C is the phase velocity, Ω is the angular frequency, and ζ_0 is the amplitude of the wave. Thus, these two modulation transfer functions are related by

$$m = (|R|/k) \tag{10}$$

where k is the wave number of the wave.

When the sea surface is described in terms of a wave height spectrum instead of a monochromatic wave, the modulation transfer function describes the relationship between the wave height spectrum and the signal spectrum measured by a radar. According to *Alpers et al.* [1981], the ratio of the SAR image spectrum $S(k_x, k_y)$ to the wave height spectrum $W(k_x, k_y)$ is equal to the square of the modulation transfer function, i.e.,

$$|R|^2 = \frac{S(k_x, k_y)}{W(k_x, k_y)} \tag{11}$$

where R includes a velocity bunching component that is assumed to be linear. However, in his Monte Carlo modeling work, W. Alpers (personal communication, 1982) appears to use a different definition for the modulation transfer function and refers to the quantity $|R|$ defined by (11) as a 'spectral mapping function.'

For the comparisons presented in this paper the definitions represented by (10) and (11) are combined to yield the one-dimensional modulation transfer function

$$m' = \frac{1}{k\bar{I}} \left[\frac{S(k)}{W(k)}\right]^{1/2} \tag{12}$$

where $\bar{I}$ is the mean signal intensity. This function is plotted versus wave number in Figure 15 for two cases, including a nearly azimuth-traveling wave and a nearly range-traveling case. Note that the modulation transfer function is smaller and falls off more rapidly with k for the azimuth-traveling wave than for the range-traveling wave. This is a direct consequence of the lower inherent modulation for azimuth-traveling waves and the degraded resolution in the azimuth direction as a result of motion effects, and it agrees, at least qualitatively, with theoretical prediction.

5. Summary

This analysis has indicated that the APD-10 SAR system imaged the dominant gravity wave component present during the MARSEN experiment, although only the first, or near-range, subswath of the APD-10 system produces reliable wave estimates. Dominant wavelength and directional information was obtainable independent of the radar look direction, although range-traveling waves are more clearly visible on the imagery than azimuth-traveling waves, based on the wave contrast criteria used in this study.

The MARSEN X band SAR data set, although limited, offers a unique opportunity to study the effect of radar look direction on the detectability of wind-generated waves and the accuracy of the SAR-derived wavelength and direction. Past studies in SAR imaging of ocean waves, such as Marineland [*Shemdin et al.*, 1978], GOASEX [*Gonzalez et al.*, 1979] and JASIN [*Vesecky et al.*, 1982], have generally shown that dominant range-traveling swell is more frequently imaged than azimuth-traveling swell and that the dominant gravity wavelength and direction is more accurately estimated for range-traveling than azimuth-traveling waves. Our MARSEN X band analysis has indicated that the accuracy of SAR-derived dominant wavelength and directional estimates is independent of radar look direction, although range-traveling waves have higher peak-to-background ratios than azimuth-traveling waves. This is probably because X band SAR data collected by a higher-velocity aircraft was used at MARSEN than at previous experiments, thus minimizing motion effects. However, the reader is cautioned to note

differences in environmental conditions as well as SAR system parameters used in these experiments.

The analysis has also indicated that the APD-10 system is relatively insensitive to wave image enhancements performed during the SAR processing. The enhancement adjustments, which are inversely proportional to the SAR platform velocity, compensate for motion of the ocean waves during the SAR observation time. Although SAR data from the APD-10 system is insensitive to the wave motion correction algorithms, numerous motion artifacts are visible on the data. These artifacts, which appear as azimuth-oriented streaks on the imagery, are more pronounced in the far subswaths. They appear to be caused by velocity variations (or coherence time) of the ocean scatterers. One possible source for these image artifacts is breaking waves.

The extraction of information on the wave height spectrum from the SAR image has also been investigated. The shape of the SAR-derived spectrum of the wave field is different from the shape of the wave spectrum obtained from surface measurements. A transfer function to relate SAR-derived spectra to in situ measurements has been developed. The transfer function is smaller for azimuth-traveling waves than for range-traveling waves, and it falls off more rapidly with wave number for the azimuth-traveling wave. This is a consequence of the smaller inherent modulation for azimuth-traveling waves and the degraded resolution in the azimuth direction as a result of motion effects, and it agrees, at least qualitatively, with theoretical predictions.

Acknowledgments. The ERIM portion of the work presented in this paper was performed under the sponsorship of the Office of Naval Research contracts N00014-76-C-1048 and N00014-81-C-0692. The technical monitor for this program was Hans Dolezalek. We thank Jack Losee and Alex Klooster of ERIM for processing the SAR data and generating the digital tapes. It is a pleasure for us to express our gratitude to a group of people involved in making this work possible, especially the two MARSEN coordinators, K. Hasselmann and O. Shemdin, and the teams from the American Air Force and the German Air Force who very generously cooperated to collect this data set.

REFERENCES

Alpers, W., and K. Hasselmann, The two-frequency technique for measuring ocean wave spectra from an airplane or satellite, *Boundary-Layer Meteorol., 13*, 215–230, 1978.

Alpers, W. E., D. B. Ross, and C. L. Rufenach, On the detectability of ocean surface waves by real and synthetic aperture radar, *J. Geophys. Res., 86*, 6481–6498, 1981.

Ausherman, D. A., W. D. Hall, J. N. Latta, and J. S. Zelenka, Radar data processing and exploitation facility, paper presented at IEEE International Radar Conference, Washington, D.C., April 21–23, 1975.

Brown, W. M., and L. Porcello, An introduction to synthetic aperture radar, *IEEE Spectrum, 6*, 52–66, 1969.

DeLoor, G. P., and P. Hoogeboom, Radar backscatter measurements from platform Noordwnijk in the North Sea, *IEEE Oceanic Eng., OE-7*, 15–20, 1982.

Forristall, G. Z., E. G. Ward, V. J. Cardone, and L. E. Borgmann, The directional spectra and kinematics of surface gravity waves in Tropical Storm Delia, *J. Phys. Oceanogr., 8*, 888–909, 1978.

Gonzalez, F. I., R. C. Beal, W. E. Brown, Jr., D. S. DeLeonibus, J. F. R. Gower, D. Lichy, D. B. Ross, C. L. Rufenach, J. W. Sherman, III, and R. A. Shuchman, Seasat synthetic aperture radar: Ocean wave detection capabilities, *Science, 204*, 1418–1421, 1979.

Gunther, H., W. Rosenthal, and M. Dunckel, The response of surface gravity waves to changing wind direction, *J. Phys. Oceanogr., 11*, 718–728, 1981.

Harger, R. O., *Synthetic Aperture Radar Systems*, 240 pp., Academic, N.Y., 1970.

Hasselmann, D. E., M. Dunckel, and J. A. Ewing, Directional wave spectra observed during JONSWAP 1973, *J. Phys. Oceanogr., 10*, 1264–1280, 1980.

Jenkins, A. M., and D. G. Watts, *Spectral Analysis and Its Applications*, 525 pp., Holden-Day, San Francisco, Calif., 1968.

Kasischke, E. S., and R. A. Shuchman, The use of wave contrast measurements in the evaluation of SAR/gravity wave models, *Proc. 15th Int. Symp. Remote Sensing Environ., 3*, 1187–1206, 1981.

Keller, W. C., and J. W. Wright, Microwave scattering and straining of wind-generated waves, *Radio Sci., 10*, 139–147, 1975.

Kinsman, B., *Wind Waves—Their Generation and Propagation on the Ocean Surface*, 676 pp., Prentice-Hall, Englewood Cliffs, N.J., 1965.

Kozma, A., E. N. Leith, and N. G. Massey, Tilted plane optical processor, *Appl. Opt., 11*, 1766–1777, 1972.

Lewis, B. L., and I. D. Olin, Experimental study and theoretical model of high-resolution backscatter from the sea, *Radio Sci., 15*, 815–828, 1980.

Long, M. W., On a two-scatter theory of sea echo, *IEEE Trans. Antennas Propagat., AP-22*, 667–672, 1974.

Longuet-Higgins, M. S., and M. D. Smith, Measurement of breaking waves by a surface jump meter, *J. Geophys. Res.*, this issue, 1983.

Lyzenga, D. R., and R. A. Shuchman, Analysis of scatterer motion effects in MARSEN *X* band SAR imagery, *J. Geophys. Res.*, this issue, 1983.

McLeish, W., D. Ross, R. A. Shuchman, P. G. Teleki, S. V. Hsiao, O. H. Shemdin, and W. E. Brown, Jr., Synthetic aperture radar imaging of ocean waves—comparison with wave measurements, *J. Geophys. Res., 85*(C9), 5003–5011, 1980.

Pawka, S. S., S. V. Hsiao, O. H. Shemdin, and O. L. Inman, Comparison between wave-directional spectra from SAR and pressure sensor arrays, *J. Geophys. Res., 85*(C9), 4987–4995, 1980.

Raney, R. K., Synthetic aperture imaging radar and moving targets, *IEEE Trans. Aerosp. Electr. Syst., AES-7*, 499–505, 1971.

Raney, R. K., SAR response to partially coherent phenomena, *IEEE Trans. Antennas Propagat., AP-28*, 777–787, 1980.

Sheffe, H., *The Analysis of Variance*, 477 pp., John Wiley, N.Y., 1959.

Shemdin, O. H., W. E. Brown, Jr., F. G. Staudhammer, R. Shuchman, R. Rawson, J. Zelenka, D. B. Ross, W. McLeish, and R. A. Berles, Comparison of in situ and remotely sensed ocean waves off Marineland, Florida, *Boundary-Layer Meterol., 13*, 193–203, 1978.

Shuchman, R. A., Processing synthetic aperture radar data of ocean waves, in *Oceanography from Space*, edited by J. F. R. Gower, pp. 477–496, Plenum, New York, 1981.

Shuchman, R. A., J. D. Lyden, and D. R. Lyzenga, Estimates of ocean wavelength and direction from X- and L-band synthetic aperture radar data collected during the Marineland experiment, *IEEE J. Oceanic Eng.*, in press, 1982.

Teleki, P. G., R. A. Shuchman, W. E. Brown, Jr., W. McLeish, D. Ross and M. Mattie, Ocean wave detection and direction measurements with microwave radars, *Oceans '78*, 639–648, 1978.

Vesecky, J. F., H. M. Assal, R. H. Stewart, R. A. Shuchman, E. S. Kasischke, and J. D. Lyden, Seasat-SAR observations of surface waves, large scale surface features and ships during the JASIN experiment, *1982 Int. Geosci. Remote Sensing Symp. Dig., 1*, 1.1–1.6, 1982.

Wright, J. W., W. J. Plant, W. C. Keller, and W. L. Jones, Ocean wave radar modulation transfer functions from the West Coast experiment, *J. Geophys. Res., 85*, 4957–4966, 1980.

(Received August 2, 1982;
revised January 12, 1983;
accepted January 12, 1983.)